Kaon photoproduction in a multipole approach

T. Mart and A. Sulaksono
Departemen Fisika, FMIPA, Universitas Indonesia, Depok 16424, Indonesia
(Received 6 June 2006; revised manuscript received 14 August 2006; published 8 November 2006)

The recently published experimental data on $K^+\Lambda$ photoproduction by the SAPHIR, CLAS, and LEPS Collaborations are analyzed by means of a multipole approach. For this purpose the background amplitudes are constructed from appropriate Feynman diagrams in a gauge-invariant and crossing-symmetric fashion. The results of our calculation emphasize the lack of mutual consistency between the SAPHIR and CLAS data previously found by several independent research groups, whereas the LEPS data are found to be more consistent with those of CLAS. The use of SAPHIR and CLAS data, individually or simultaneously, leads to quite different resonance parameters that, therefore, could lead to different conclusions on "missing resonances." Fitting to the SAPHIR and LEPS data simultaneously indicates that the $S_{11}(1650)$, $P_{13}(1720)$, $D_{13}(1700)$, $D_{13}(2080)$, $F_{15}(1680)$, and $F_{15}(2000)$ resonances are required, whereas fitting to the combination of CLAS and LEPS data leads alternatively to the $P_{13}(1900)$, $D_{13}(2080)$, $D_{15}(1675)$, $F_{15}(1680)$, and $F_{17}(1990)$ resonances. Although yielding different results in most cases, both SAPHIR and CLAS data indicate that the second peak in the cross sections at $W \sim 1900$ MeV originates from the $D_{13}(2080)$ resonance with a mass between 1911 and 1936 MeV. Furthermore, in contrast to the results of currently available models and the Table of Particle Properties, both data sets do not exhibit the need for a $P_{11}(1710)$ resonance. The few data points available for target asymmetry cannot be described by the models proposed in the present work.

DOI: 10.1103/PhysRevC.74.055203 PACS number(s): 13.60.Le, 25.20.Lj, 14.20.Gk

I. INTRODUCTION

Modern theories of the strong interaction would certainly be incomplete if we ignored the necessity to understand hadronic interactions in the medium energy region. However, due to the nonperturbative nature of quantum chromodynamics (QCD) at these energies, hadronic physics continues to be a challenging field of investigation. This is also supported by the fact that methods like chiral perturbation theory are not amenable to this energy region. Lattice QCD, which is expected to alleviate this problem, has only recently begun to contribute to this field.

One of the most intensively studied topics in the realm of hadronic physics is the associated strangeness photoproduction. High-intensity continuous electron beams produced by modern accelerator technologies, along with unprecedented precise detectors, are among the important aspects that have brought renewed attention to this 40-year-old field of research. However, the argument that some of the resonances predicted by constituent quark models are strongly coupled to strangeness channels, and therefore intangible to $\pi N \to \pi N$ reactions that are used by Particle Data Group (PDG) to extract the properties of nucleon resonances, has raised the issue of "missing" resonances. As a consequence, photoproduction of strange particles becomes a unique tool that can shed important information on the structure of resonances and, thus, complement the $\pi N \to \pi N$ channels. Among the possible reactions, the $\gamma p \to K^+\Lambda$ is the most intensively studied channel because it does not involve isospin-3/2 intermediate states, which makes theoretical formalism much simpler. It is also this channel for which most of the good-quality experimental data are available. Furthermore, in this process the self-analyzing power of the weak decay $\Lambda \to p\pi^-$ can be utilized to determine the polarization of the recoiled Λ. Therefore, the beauty of working with $K^+\Lambda$ photoproduction is that precise Λ polarizations will accompany accurate cross-section measurements.

Over the past few decades a large number of attempts have been devoted to modeling the above reaction process. Most of these have been performed in the framework of tree-level isobar models [1–5], coupled-channels calculations [6–8], or quark models [9,10]. Extending the validity of isobar models to higher energy regions has also been recently pursued [11–13].

In contrast to pion and eta photoproduction, the kaon photoproduction process is not dominated by a single resonant state. Therefore, the main difference among the models is chiefly in the use of nucleon, hyperon, and kaon resonances. The widely used KAON-MAID model [5], for instance, uses nucleon resonances $S_{11}(1650)$, $P_{11}(1710)$, $P_{13}(1720)$, and $D_{13}(1895)$, where the latter is known as the missing resonance in this model. However, the Adelseck-Saghai model [2] has solely one nucleon resonance $S_{11}(1650)$ and one hyperon resonance $S_{01}(1670)$. The more complicated Saclay-Lyon model [14] utilizes the $P_{11}(1440)$, $P_{13}(1720)$, and $D_{15}(1675)$ nucleon resonances, along with the $S_{01}(1405)$, $S_{01}(1670)$, $P_{01}(1810)$, and $P_{11}(1660)$ hyperon resonances. Although those models vary with the number of resonances, they mostly use low-spin states, because higher spin propagators and vertices are quite complicated in such a framework and, moreover, are not free of some fundamental ambiguities. Only in the Saclay-Lyon [14] and Renard-Renard models [15] is a spin-5/2 nucleon resonance utilized. Other models argue that the use of resonance excitation up to spin 3/2, or even up to spin 1/2, is sufficient.

Clearly, there is a lack of a systematic procedure to determine how many resonances should be built into the process. There has been no attempt to include the F_{15}, F_{17}, G_{17}, and G_{19} states, although some of them could have sizable branching

fractions to the $K\Lambda$ channel (see Table II in the next section or *Review of Particle Properties* [16]).

The main motivation of the present work is to explore the possibility of using higher spin states in kaon photoproduction. Ideally, this should be performed on the basis of a coupled-channels formalism. However, the level of complexity in such a framework increases quickly with the addition of resonance states. In view of this, we constrain the present work to a single-channel analysis, but we use as much as possible nucleon resonances listed by PDG. This argument is also supported by the fact that the recently available SAPHIR [17] and CLAS [18] data have a problem of mutual consistency [7,19]. Thus, another purpose of this work is to investigate the physics consequence of using each data set. The present work is basically an extension of our previous analysis [20], which was performed using a slightly different method and only the SAPHIR data [17]. To this end, we use the same formalism developed for pion photoproduction [21,22], which has the advantage that it provides a direct comparison of the extracted helicity photon coupling with the PDG values and paves the way for extending the present work to incorporate the effect of other related channels.

This article is organized as follows. In Sec. II we present the formalism of our work. Section III briefly discusses the experimental data used in the fitting process as well as the chosen fitting strategy. In Sec. IV we discuss the comparison of the results of our calculation with the current available data. In this section we also discuss the possible origin of the second peak in the cross sections at $W \sim 1900$ MeV. In Sec. V we summarize our findings.

II. FORMALISM

A. The background amplitudes

The background amplitudes are obtained from a series of tree-level Feynman diagrams [23]. They consist of the standard s-, u-, and t-channel Born terms along with the $K^*(892)$ and $K_1(1270)$ t-channel vector mesons. Altogether they are often called extended Born terms. Apart from the $K_1(1270)$ exchange, these background terms are similar to the ones used by Thom [24]. The importance of the $K_1(1270)$ intermediate state has been pointed out for the first time by Ref. [25] and since then it has been extensively used in almost all isobar models. To account for hadronic structures of interacting baryons and mesons we include the appropriate hadronic form factors in the hadronic vertices by utilizing the method developed by Haberzettl to maintain gauge invariance of the amplitudes. We have also tested the gauge method proposed by Ohta [26], but because the produced χ^2 is substantially larger, we do not discuss the Ohta method here. Furthermore, to comply with the *crossing symmetry* requirement we use a special form factor in the *gauge terms*

$$\begin{aligned}\widehat{F}(s,t,u) = {} & F_1(s) + F_1(u) + F_3(t) - F_1(s)F_1(u) \\ & - F_1(s)F_3(t) - F_1(u)F_3(t) + F_1(s)F_1(u)F_3(t),\end{aligned} \tag{1}$$

proposed by Davidson and Workman [27], with Mandelstam variables s, t, and u, and

$$F_i(x) = \frac{\Lambda^4}{\Lambda^4 + \left(x - m_i^2\right)^2}, \tag{2}$$

where Λ and m_i are the form factor cutoff and the intermediate state mass, respectively [28]. Thus, compared to the previous pioneering work [24], the major improvement in the background sector is the use of hadronic form factors in a gauge-invariant fashion and the crossing-symmetric properties of the Born terms.

B. The resonance amplitudes

The resonant electric and magnetic multipoles for a state with the mass M_R, width Γ, and angular momentum ℓ are assumed to have the Breit-Wigner form [21,22]

$$A^R_{\ell\pm}(W) = \bar{A}^R_{\ell\pm} c_{\rm KY} \frac{f_{\gamma R}(W)\,\Gamma_{\rm tot}(W) M_R f_{\rm KR}(W)}{M_R^2 - W^2 - i M_R \Gamma_{\rm tot}(W)}\, e^{i\phi}, \tag{3}$$

where W represents the total center-of-momentum (c.m.) energy, the isospin factor $c_{\rm KY}$ is -1 [29], and $f_{\rm KR}$ is the usual Breit-Wigner factor describing the decay of a resonance R with a total width $\Gamma_{\rm tot}(W)$ and physical mass M_R. The $f_{\gamma R}$ indicates the γNR vertex and ϕ represents the phase angle. The Breit-Wigner factor $f_{\rm KR}$ is given by

$$\begin{aligned} f_{\rm KR}(W) &= \left[\frac{1}{(2j+1)\pi}\frac{k_W}{|\boldsymbol{q}|}\frac{m_N}{W}\frac{\Gamma_{\rm KY}}{\Gamma_{\rm tot}^2}\right]^{1/2}, \\ k_W &= \frac{W^2 - m_N^2}{2W}, \end{aligned} \tag{4}$$

with m_N representing the nucleon mass. The energy-dependent partial width $\Gamma_{\rm KY}$ is defined through

$$\Gamma_{\rm KY} = \beta_K \Gamma_R \left(\frac{|\boldsymbol{q}|}{q_R}\right)^{2\ell+1} \left(\frac{X^2 + q_R^2}{X^2 + \boldsymbol{q}^2}\right)^{\ell} \frac{W_R}{W}, \tag{5}$$

where the damping parameter X is assumed to be 500 MeV for all resonances, β_K is the single-kaon branching ratio, and Γ_R and q_R are the total width and kaon c.m. momentum at $W = M_R$. The γNR vertex is parametrized through

$$f_{\gamma R} = \left(\frac{k_W}{k_R}\right)^{2\ell'+1} \left(\frac{X^2 + k_R^2}{X^2 + k_W^2}\right)^{\ell'}, \tag{6}$$

where k_R is equal to k_W calculated at $W = M_R$. For $M_{\ell\pm}$ and $E_{\ell+}$: $\ell' = \ell$, whereas for $E_{\ell-}$: $\ell' = \ell - 2$ if $\ell \geqslant 2$ [30]. The values of ℓ and ℓ' for all resonances considered in this study are given in Table I.

The total width appearing in Eqs. (3) and (4) is the sum of Γ_K and the "inelastic" width $\Gamma_{\rm in}$. In this work we assume the dominance of the pion decay channel and we parametrize the width by using

$$\begin{aligned} \Gamma_{\rm tot} &= \Gamma_{\rm KY} + \Gamma_{\rm in}, \\ \Gamma_{\rm in} &= (1 - \beta_K)\Gamma_R \left(\frac{q_\pi}{q_0}\right)^{2\ell+4} \left(\frac{X^2 + q_0^2}{X^2 + q_\pi^2}\right)^{\ell+2}, \end{aligned} \tag{7}$$

TABLE I. The electric and magnetic multipole photon couplings in terms of the helicity photon couplings for resonances up to $\ell = 4$.

Resonance	ℓ	ℓ'	Multipoles	Expression
S_{11}	0	0	$\bar{E}_{0+}$	$-A^{0+}_{1/2}$
P_{11}	1	1	$\bar{M}_{1-}$	$A^{1-}_{1/2}$
P_{13}	1	1	$\bar{E}_{1+}$	$\frac{1}{2}\left(-A^{1+}_{1/2}+\sqrt{\frac{1}{3}}A^{1+}_{3/2}\right)$
	1	1	$\bar{M}_{1+}$	$-\frac{1}{2}\left(A^{1+}_{1/2}+\sqrt{3}A^{1+}_{3/2}\right)$
D_{13}	2	0	$\bar{E}_{2-}$	$-\frac{1}{2}\left(A^{2-}_{1/2}+\sqrt{3}A^{2-}_{3/2}\right)$
	2	2	$\bar{M}_{2-}$	$\frac{1}{2}\left(A^{2-}_{1/2}-\sqrt{\frac{1}{3}}A^{2-}_{3/2}\right)$
D_{15}	2	2	$\bar{E}_{2+}$	$\frac{1}{3}\left(-A^{2+}_{1/2}+\sqrt{\frac{1}{2}}A^{2+}_{3/2}\right)$
	2	2	$\bar{M}_{2+}$	$-\frac{1}{3}\left(A^{2+}_{1/2}+\sqrt{2}A^{2+}_{3/2}\right)$
F_{15}	3	1	$\bar{E}_{3-}$	$-\frac{1}{3}\left(A^{3-}_{1/2}+\sqrt{2}A^{3-}_{3/2}\right)$
	3	3	$\bar{M}_{3-}$	$\frac{1}{3}\left(A^{3-}_{1/2}-\sqrt{\frac{1}{2}}A^{3-}_{3/2}\right)$
F_{17}	3	3	$\bar{E}_{3+}$	$\frac{1}{4}\left(-A^{3+}_{1/2}+\sqrt{\frac{3}{5}}A^{3+}_{3/2}\right)$
	3	3	$\bar{M}_{3+}$	$-\frac{1}{4}\left(A^{3+}_{1/2}+\sqrt{\frac{5}{3}}A^{3+}_{3/2}\right)$
G_{17}	4	2	$\bar{E}_{4-}$	$-\frac{1}{4}\left(A^{4-}_{1/2}+\sqrt{\frac{5}{3}}A^{4-}_{3/2}\right)$
	4	4	$\bar{M}_{4-}$	$\frac{1}{4}\left(A^{4-}_{1/2}-\sqrt{\frac{3}{5}}A^{4-}_{3/2}\right)$
G_{19}	4	4	$\bar{E}_{4+}$	$\frac{1}{5}\left(-A^{4+}_{1/2}+\sqrt{\frac{2}{3}}A^{4+}_{3/2}\right)$
	4	4	$\bar{M}_{4+}$	$-\frac{1}{5}\left(A^{4+}_{1/2}+\sqrt{\frac{3}{2}}A^{4+}_{3/2}\right)$

with q_π the momentum of the π in the decay of $R \to \pi + N$ in c.m. system and $q_0 = q_\pi$ calculated at $W = M_R$.

The electric and magnetic multipole photon couplings $\bar{A}^R_{\ell\pm}$ in Eq. (3) can be related to the helicity photon couplings $A_{1/2}$ and $A_{3/2}$. For resonances with total spin $j = \ell + 1/2$ we get [22]

$$A^{\ell+}_{1/2} = -\tfrac{1}{2}[(\ell+2)\bar{E}_{\ell+} + \ell\bar{M}_{\ell+}], \tag{8}$$

$$A^{\ell+}_{3/2} = \tfrac{1}{2}\sqrt{\ell(\ell+2)}(\bar{E}_{\ell+} - \bar{M}_{\ell+}), \tag{9}$$

and for $j = (\ell+1) - 1/2$

$$A^{(\ell+1)-}_{1/2} = \tfrac{1}{2}[(\ell+2)\bar{M}_{(\ell+1)-} - \ell\bar{E}_{(\ell+1)-}], \tag{10}$$

$$A^{(\ell+1)-}_{3/2} = -\tfrac{1}{2}\sqrt{\ell(\ell+2)}[\bar{E}_{(\ell+1)-} + \bar{M}_{(\ell+1)-}]. \tag{11}$$

Equations (8)–(11) can be inverted to give the electric and magnetic multipole photon couplings in terms of the helicity photon couplings as

$$\bar{E}_{\ell+} = \frac{1}{\ell+1}\left(-A^{\ell+}_{1/2} + \sqrt{\frac{\ell}{\ell+2}}A^{\ell+}_{3/2}\right), \tag{12}$$

$$\bar{M}_{\ell+} = -\frac{1}{\ell+1}\left(A^{\ell+}_{1/2} + \sqrt{\frac{\ell+2}{\ell}}A^{\ell+}_{3/2}\right), \tag{13}$$

for $j = \ell + 1/2$ and

$$\bar{E}_{(\ell+1)-} = -\frac{1}{\ell+1}\left[A^{(\ell+1)-}_{1/2} + \sqrt{\frac{\ell+2}{\ell}}A^{(\ell+1)-}_{3/2}\right], \tag{14}$$

$$\bar{M}_{(\ell+1)-} = \frac{1}{\ell+1}\left[A^{(\ell+1)-}_{1/2} - \sqrt{\frac{\ell}{\ell+2}}A^{(\ell+1)-}_{3/2}\right], \tag{15}$$

for $j = (\ell+1) - 1/2$. All relevant multipole photon couplings used in this work are given in Table II.

All observables can be calculated from the Chew-Goldberger-Low-Nambu (CGLN) amplitudes [31]

$$F = i\boldsymbol{\sigma}\cdot\boldsymbol{\epsilon}F_1 + \boldsymbol{\sigma}\cdot\hat{\boldsymbol{q}}\,\boldsymbol{\sigma}\cdot(\hat{\boldsymbol{k}}\times\boldsymbol{\epsilon})F_2 + i\boldsymbol{\sigma}\cdot\hat{\boldsymbol{k}}\,\hat{\boldsymbol{q}}\cdot\boldsymbol{\epsilon}F_3 + i\boldsymbol{\sigma}\cdot\hat{\boldsymbol{q}}\,\hat{\boldsymbol{q}}\cdot\boldsymbol{\epsilon}F_4, \tag{16}$$

TABLE II. Resonances up to $\ell = 4$ with the corresponding properties from the *Review of Particle Properties* [16].

Resonance	M_R (MeV)	Γ_R (MeV)	β_K	$A_{1/2}(p)$ (10^{-3} GeV$^{-1/2}$)	$A_{3/2}(p)$ (10^{-3} GeV$^{-1/2}$)	Overall status	Status seen in $K\Lambda$
S_{11}	1650	150	0.027 ± 0.004	$+53 \pm 16$	—	****	***
	2090	400	—	—	—	*	—
P_{11}	1710	100	0.050 ± 0.020	$+9 \pm 22$	—	***	**
	2100	200	—	—	—	*	—
P_{13}	1720	150	—	$+18 \pm 30$	-19 ± 20	****	**
	1900	498	0.001 ± 0.001	—	—	**	—
D_{13}	1700	100	—	-18 ± 13	-2 ± 24	***	**
	2080	450	0.002 ± 0.002	-20 ± 8	17 ± 11	**	*
D_{15}	1675	150	—	$+19 \pm 8$	15 ± 9	****	*
	2200	130	—	—	—	**	*
F_{15}	1680	130	—	-15 ± 6	133 ± 12	****	—
	2000	490	—	—	—	**	*
F_{17}	1990	535	—	$+30 \pm 29$	86 ± 60	**	*
G_{17}	2190	450	—	-55	$+81$	****	*
G_{19}	2250	400	—	—	—	****	—

where the amplitudes F_i are related to the electric and magnetic multipoles given in Eq. (3) for up to $\ell = 4$ by

$$\begin{aligned}
F_1 &= E_{0+} - \tfrac{3}{2}(E_{2+} + 2M_{2+}) + E_{2-} + 3M_{2-} \\
&\quad + \tfrac{15}{8}(E_{4+} + 4M_{4+}) - \tfrac{3}{2}(E_{4-} + 5M_{4-}) \\
&\quad + 3\big[E_{1+} + M_{1+} - \tfrac{5}{2}(E_{3+} + 3M_{3+}) + E_{3-} + 4M_{3-}\big] \\
&\quad \times \cos\theta + \tfrac{15}{2}\big[E_{2+} + 2M_{2+} - \tfrac{7}{2}(E_{4+} + 4M_{4+}) \\
&\quad + E_{4-} + 5M_{4-}\big]\cos^2\theta + \tfrac{35}{2}(E_{3+} + 3M_{3+})\cos^3\theta \\
&\quad + \tfrac{315}{8}(E_{4+} + 4M_{4+})\cos^4\theta, \qquad (17) \\
F_2 &= 2M_{1+} + M_{1-} - \tfrac{3}{2}(4M_{3+} + 3M_{3-}) \\
&\quad + 3\big[3M_{2+} + 2M_{2-} - \tfrac{5}{2}(5M_{4+} + 4M_{4-})\big]\cos\theta \\
&\quad + \tfrac{15}{2}(4M_{3+} + 3M_{3-})\cos^2\theta + \tfrac{35}{2}(5M_{4+} + 4M_{4-}) \\
&\quad \times \cos^3\theta, \qquad (18) \\
F_3 &= 3\big[E_{1+} - M_{1+} - \tfrac{5}{2}(E_{3+} - M_{3+}) + E_{3-} + M_{3-}\big] \\
&\quad + 15\big[E_{2+} - M_{2+} + E_{4-} + M_{4-} - \tfrac{7}{2}(E_{4+} - M_{4+})\big] \\
&\quad \times \cos\theta + \tfrac{105}{2}(E_{3+} - M_{3+})\cos^2\theta \\
&\quad + \tfrac{315}{2}(E_{4+} - M_{4+})\cos^3\theta, \qquad (19) \\
F_4 &= 3\big[M_{2+} - E_{2+} - M_{2-} - E_{2-} \\
&\quad - \tfrac{5}{2}(M_{4+} - E_{4+} - M_{4-} - E_{4-})\big] \\
&\quad + 15(M_{3+} - E_{3+} - M_{3-} - E_{3-})\cos\theta \\
&\quad + \tfrac{105}{2}(M_{4+} - E_{4+} - M_{4-} - E_{4-})\cos^2\theta. \qquad (20)
\end{aligned}$$

These amplitudes are combined with the CGLN amplitudes obtained from the background terms discussed in Sec. II A.

III. EXPERIMENTAL DATA AND FITTING STRATEGY

A. Experimental data

All experimental data used in the present analysis are summarized in Table III. The 2004 SAPHIR differential cross-section data are given in 36 angular distributions with ∼20-MeV energy bins, spanning from reaction threshold up to $W = 2.4$ GeV. The obtained differential cross sections are represented in 20 panels showing energy distributions. The recoil polarization is also given in five angular bins.

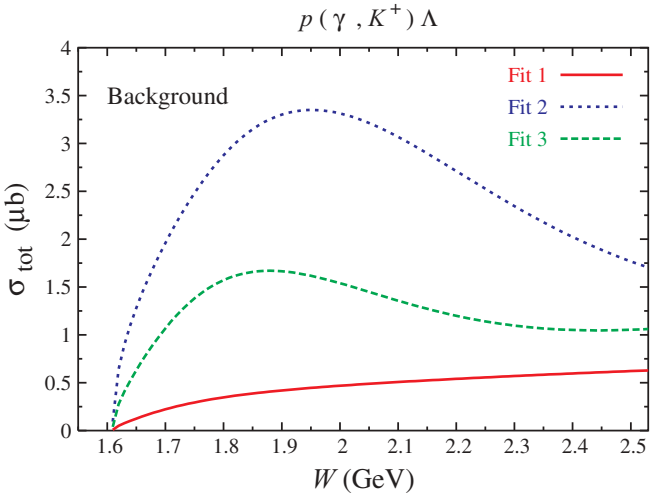

FIG. 1. (Color online) Contributions from the background amplitudes to the total cross sections for all fits.

The latest version of the CLAS data [18] covers almost the same energy range, from threshold up to about 2.5 GeV, but are given in 76 bins of angular distributions, with a step size in E_γ of 25 MeV, or about 9–14 MeV in W, covering 18 angular bins in W excitations. The recoil polarization data are taken from the previous data analysis [32], which are presented in 29 angular distributions. In addition, both SAPHIR and CLAS present figures of total cross sections but do not give tables of numerical values. In our analysis we did not use these data in the fits, but we show these for the sake of comparison.

The LEPS collaboration reported the SPRING8 data in terms of differential cross sections and photon asymmetries at forward kaon angles [33]. These data are used in our analysis.

In addition, we also compare the three data points from an old measurement of the target asymmetry [34] with our results. These data have been recently used by several authors [7,14,35,36].

Because several recent studies have reported the problem of mutual consistency between SAPHIR and CLAS data [7,19], in our database we define three different data sets, as shown in Table III. In the first fit (Fit 1) we use only SAPHIR and LEPS

TABLE III. Experimental data sets used in the present analysis. Experimental data set used in the individual fits are indicated by √. Otherwise, data are only used for comparison.

Name	Observable	Symbol	N	Fit 1	Fit 2	Fit 3	Ref.
SAPHIR 2004	Differential cross section	$d\sigma/d\Omega$	720	√	—	√	[17]
	Recoil polarization	P	30	√	—	√	[17]
	Total cross section	$\sigma_{\rm tot}$	36	—	—	—	[17]
CLAS 2006	Differential cross section	$d\sigma/d\Omega$	1377	—	√	√	[18]
	Recoil polarization	P	233	—	√	√	[18]
	Total cross section	$\sigma_{\rm tot}$	78	—	—	—	[18]
LEPS 2006	Differential cross section	$d\sigma/d\Omega$	54	√	√	√	[33]
	Photon asymmetry	Σ	30	√	√	√	[33]
OLD	Target asymmetry	T	3	—	—	—	[34]
	Total cross section	$\sigma_{\rm tot}$	24	—	—	—	[39]
Total data				834	1694	2444	

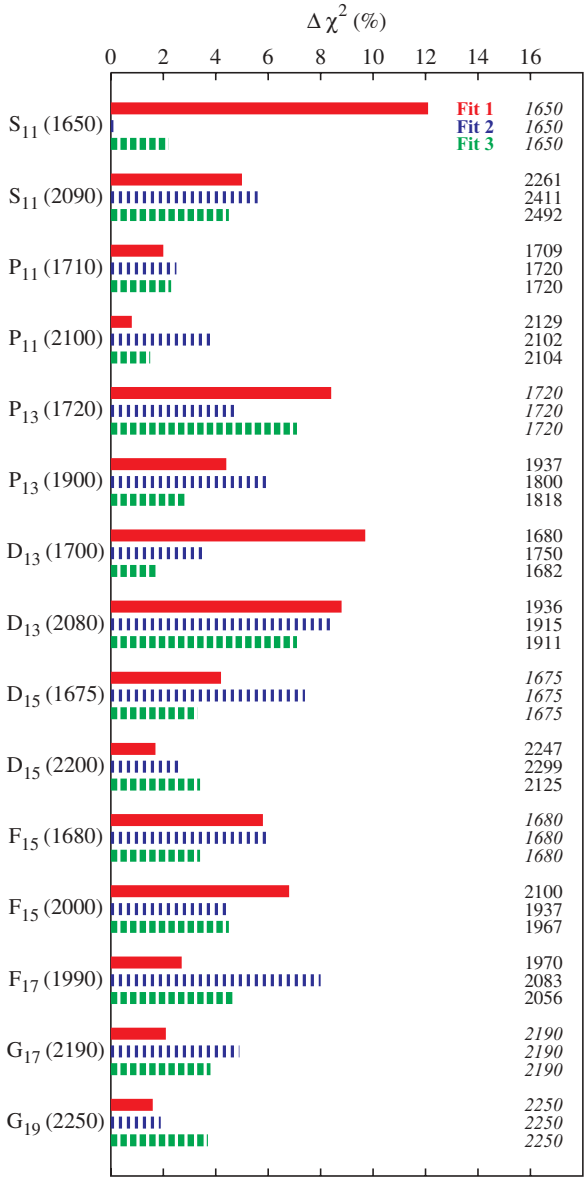

FIG. 2. (Color online) The significance of individual resonances in the three different fits. Values written in italic were fixed during the fit process.

data, whereas in the second one (Fit 2) we use a combination of CLAS and LEPS data. In the last one (Fit 3) we use all data (SAPHIR, CLAS, and LEPS) in the fit.

Note that we do not use the old data in any fit, because Ref. [19] has pointed out that some of them (old SAPHIR data) are consistent only with the new SAPHIR data, whereas some others (much older measurements [37]) are consistent only with the CLAS data.

B. Fitting strategy

Recent analyses of kaon photoproduction have focused mostly on the quest of missing resonances. With the new CLAS data appearing this year [18], this becomes an arduous task, because Ref. [19] found a lack of mutual consistency between the recent CLAS and SAPHIR data. As shown in the next section, the use of the two data sets, individually or simultaneously, leads to quite different values of the extracted resonance parameters and, therefore, could yield different conclusions on the missing resonances studied by this reaction. In view of this, in the present work we do not focus our attention on searching for missing resonances. Instead, we use all nucleon resonances listed by PDG up to spin 9/2 and fit their parameters to new data. Along with their known parameters those resonances are listed in Table II. Note that we do not use resonances with masses below the reaction threshold (1610 MeV) because their contributions would contribute only to the background terms and therefore would be difficult to see in the present formalism. Furthermore, we do not include the two resonances with spins higher than 9/2 (i.e., I_{111} and K_{113}) for practical reasons and because too little information is available for both states.

The number of free parameters is relatively large, i.e., 7 from the background amplitude and 86 from the resonance part. To reduce this we fix both $g_{K\Lambda N}$ and $g_{K\Sigma N}$ coupling constants to the SU(3) predictions, i.e., $g_{K\Lambda N}/\sqrt{4\pi} = -3.80$ and $g_{K\Sigma N}/\sqrt{4\pi} = 1.20$, and fix masses as well as widths of the four-star resonances to their PDG values. To avoid unrealistically large values obtained from fitting to experimental data, the total width Γ_R is limited to 500 MeV and the kaon branching ratio β_K is limited to 0.3. The χ^2 minimization fit is performed by using the CERN-MINUIT code.

IV. RESULTS AND DISCUSSION

A. Numerical results

Contributions to the χ^2 from individual data for all fits are given in Table IV. By comparing the contributions for Fit 1 and Fit 2 it is clear that the LEPS data are more compatible with the CLAS rather than with the SAPHIR measurement. It is also apparent that, in spite of the large number of data, the CLAS differential cross sections (74%) are internally more consistent than the SAPHIR ones (84%). These results corroborate the finding of Ref. [19]. Of course, the situation significantly changes when all data are simultaneously used in the fit, i.e., because the CLAS error bars are in general smaller than those of SAPHIR, the CLAS differential cross sections contribute more to the χ^2 than the SAPHIR ones.

The extracted background parameters are shown in Table V. In this case it is interesting to note the different values in the

TABLE IV. Contribution to χ^2 (in %) from individual data sets for the three different fits.

Name	Observable	N	Fit 1	Fit 2	Fit 3
SAPHIR 2004	Differential cross section	720	84	—	39
	Recoil polarization	30	3	—	1
CLAS 2006	Differential cross section	1377	—	74	45
	Recoil polarization	233	—	17	9
LEPS 2006	Differential cross section	54	10	7	5
	Photon asymmetry	30	3	2	1

TABLE V. The extracted coupling constants, hadronic form factor cutoffs (Λ), number of data (N), and χ^2 per number of degrees of freedom from the three different fits.

	$\frac{G_V(K^*)}{4\pi}$	$\frac{G_T(K^*)}{4\pi}$	$\frac{G_V(K_1)}{4\pi}$	$\frac{G_T(K_1)}{4\pi}$	Λ (GeV)	N	χ^2	$\chi^2/N_{\rm dof}$
Fit 1	1.19 ± 0.19	-3.57 ± 0.48	0.18 ± 0.32	-4.95 ± 1.23	0.50 ± 0.02	834	772	1.02
Fit 2	0.06 ± 0.00	-0.18 ± 0.01	0.16 ± 0.01	-1.13 ± 0.02	1.13 ± 0.01	1694	1581	0.98
Fit 3	-0.02 ± 0.01	-0.64 ± 0.04	0.71 ± 0.04	-1.94 ± 0.07	0.91 ± 0.02	2444	3095	1.31

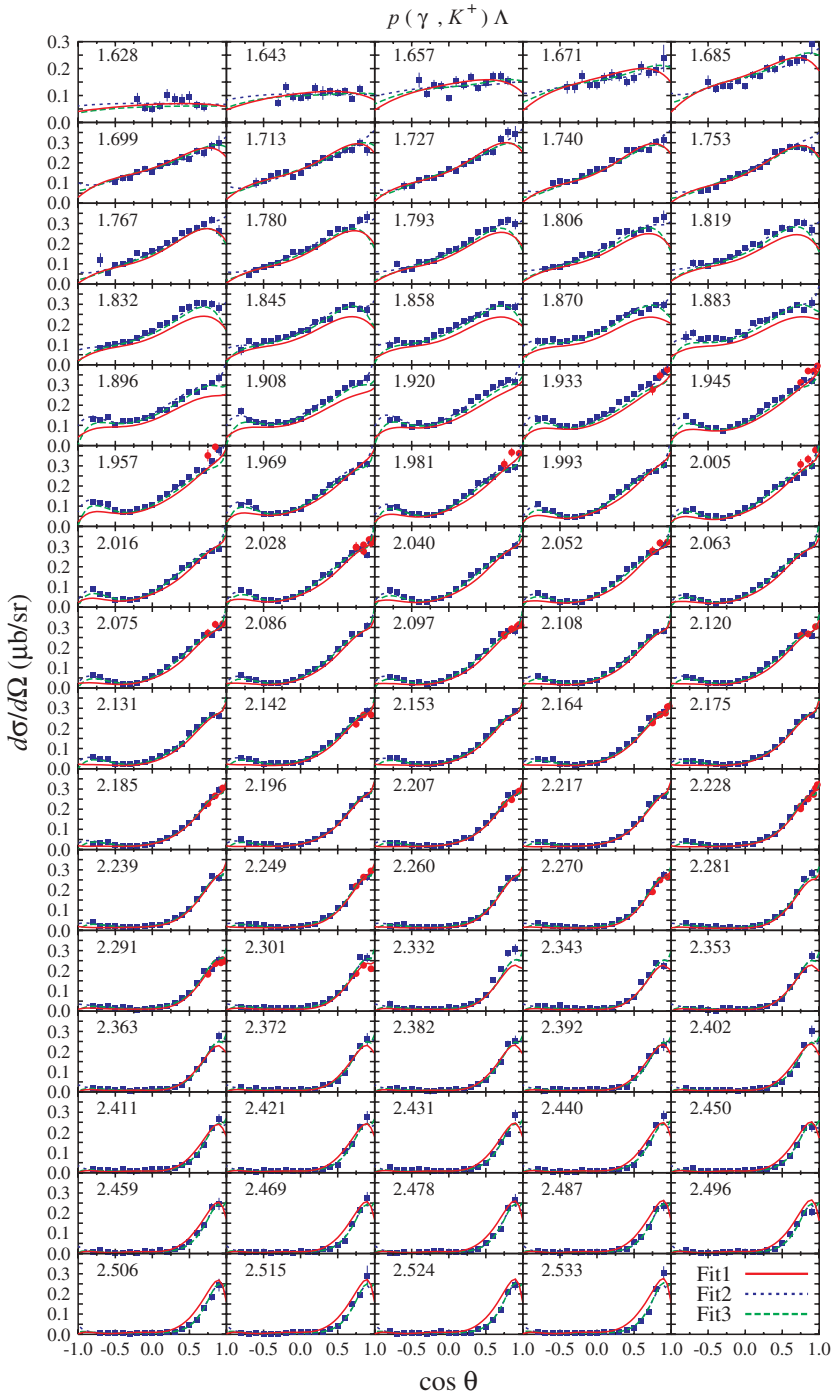

FIG. 3. (Color online) Comparison between angular distribution of differential cross sections obtained from the three fits with CLAS (solid squares) and LEPS (solid circles) data.

vector mesons coupling constants extracted from different sets of data. Obviously, fitting to the CLAS and LEPS data results in smaller coupling constants. However, the corresponding hadronic form factor cutoff is significantly larger than that obtained in Fit 1. Including all data sets in the database leads to a compromise result, i.e., the extracted parameters basically lie between those obtained from Fit 1 and Fit 2. To investigate the qualitative effect of these parameters on the observable, in Fig. 1 we compare contributions of the background terms to the total cross sections of all fits. Obviously, the different values of coupling constants lead to different-size backgrounds. For Fit 1, the large coupling constants combined with the soft form factor cutoff yields a small background that systematically increases as a function of W. On the contrary, the relatively hard hadronic form factor cutoff in Fit 2 is unable to suppress the large contribution of the standard Born terms and, therefore, yields a large background. Although tending to be convergent at higher energies, such a large background seems to be unrealistic if we compare it to the experimental total cross section data. This indicates that the extracted hadronic form factor cutoff (i.e., $\Lambda = 1.13$ GeV) is presumably too large for kaon photoproduction. A similar result has been found in the isobar model of Ref. [36], where a value of $\Lambda = 0.80$ GeV is demanded. As expected, a compromise background will be obtained if we use all data sets.

Because in general the error bars of CLAS data are smaller than those of SAPHIR data, the smaller value of $\chi^2/N_{\rm dof}$ exhibited by Fit 2 in Table V again indicates that the CLAS data show a better internal consistency than the SAPHIR data, a point that has been discussed previously.

The extracted resonance parameters for all three different fits are shown in Table VI. The agreements with the PDG values are mostly good or fair and for some resonances there are significant discrepancies. Because in this framework (single-channel analysis) we are unable to consider the effect of other channels that could substantially influence the widths, photon couplings, and branching fractions of those resonances, we only qualitatively discuss the variation of certain resonance parameters obtained for the three different fits. A more detailed study, in which these parameters are constrained within the PDG values and all information from other related channels (i.e., $\pi N, \pi\pi N, \eta N$) is taken into account in the inelastic width of Eq. (7), will be reported in a future publication [38].

The first resonance of interest is $P_{11}(1710)$, for which the extracted masses and widths from all fits are in agreement with the PDG values. In the case of Fit 1 the extracted helicity photon coupling is also in agreement with the PDG $A_{1/2}$ value. The second resonance is the $P_{11}(2100)$, for which fitting to SAPHIR or CLAS data leads to a mass that is in good agreement with the PDG value, whereas, however, the extracted width underpredicts the PDG value by almost 50%. In the case of Fit 2 this resonance is required to explain a small bump in the cross sections around 2150 MeV. This bump seems to be very tiny in the SAPHIR differential cross-section data, but it is still visible in the total cross sections. The third resonance is the $D_{13}(2080)$, for which all three fits clearly underestimate the PDG mass. This is discussed in the Sec. IV B. The fourth resonance is the $F_{15}(2000)$. In this case SAPHIR data demand this resonance to explain the small peak at $W \sim 2150$ MeV, whereas CLAS data require it to describe the second peak around $W \sim 1900$ MeV. The last resonance is the $F_{17}(1990)$ for which SAPHIR data lead to resonance parameters that are in a fair agreement (up to the sign of the photon couplings) with PDG values, whereas CLAS data overestimate the PDG mass.

To further investigate the importance of the individual resonances we define a parameter

$$\Delta\chi^2 = \frac{\chi^2_{\rm All} - \chi^2_{{\rm All}-N^*}}{\chi^2_{\rm All}} \times 100\%, \tag{21}$$

where $\chi^2_{\rm All}$ is the χ^2 obtained by using all resonances and $\chi^2_{{\rm All}-N^*}$ is the χ^2 obtained by using all but a specific resonance. Therefore, $\Delta\chi^2$ measures the relative difference between the χ^2 of including and of excluding the corresponding resonance. Note that the $\Delta\chi^2$ does not measure the "strength" of the resonance in the process but it merely reveals information on how difficult to reproduce experimental data without that resonance. A similar ratio has been also defined in Ref. [7] to investigate the role of individual resonances. The numerical result is listed in the last column of Table VI. However, the result would be more clear if displayed in a histogram shown in Fig. 2. Except for the $S_{11}(2090)$, $P_{11}(1710)$, $D_{13}(2080)$, $F_{15}(1680)$, and $G_{19}(2250)$, for which the $\Delta\chi^2$ are almost similar, the histogram shows that the new CLAS and SAPHIR data can be explained only by different sets of nucleon resonances. If we, for instance, trivially define the important resonances as those with $\Delta\chi^2 \gtrsim 6\%$, in other words we pick about 30% out of all resonances used in both Fit 1 and Fit 2, then the important resonances in Fit 1 are the $S_{11}(1650)$, $P_{13}(1720)$, $D_{13}(1700)$, $D_{13}(2080)$, $F_{15}(1680)$, and $F_{15}(2000)$, whereas Fit 2 requires the $P_{13}(1900)$, $D_{13}(2080)$, $D_{15}(1675)$, $F_{15}(1680)$, and $F_{17}(1990)$. However, fitting all data simultaneously yields a compromise result and changes this conclusion, which indicates that the corresponding result is neither consistent with Fit 1 nor with Fit 2.

It is interesting to note here that both Fit 1 and Fit 2 support the requirement of $D_{13}(2080)$ in the $K^+\Lambda$ production process. Surprisingly, all new data reject the need for the $P_{11}(1710)$, and the new CLAS data do not require the contribution from the $P_{13}(1720)$ resonance. However, most recent analyses of the $K^+\Lambda$ channel have included these intermediate states. Another new phenomenon is the contribution from $F_{15}(2000)$ and $F_{17}(1900)$, which are quite important according to SAPHIR and CLAS data, respectively. These resonances have not been used in most analyses, especially in the isobar model with diagrammatic technique, because in this approach not only are the propagators for spins 5/2 and 7/2 quite complicated but also their forms are not unique.

Except for the $F_{17}(1990)$ resonance, the importance of individual resonances discussed above is generally confirmed by the reasonable error bars of the fitted parameters shown in Table VI. In the case of $F_{17}(1990)$ the error bar of the kaon branching ratio β_K is almost the same as the value of β_K itself, whereas the corresponding $\Delta\chi^2$ indicates that this resonance is strongly needed to explain the CLAS data. We have tried to understand this by relaxing the upper limit of β_K and refitting the $F_{17}(1990)$ resonance parameters. It is found that with the

TABLE VI. The extracted resonance parameters from the three different fits. Values written in italic were fixed during the fitting process.

Resonance (status)	M_R (MeV)	Γ_R (MeV)	$A_{1/2}$ (10^{-3} GeV$^{-1/2}$)	$A_{3/2}$ (10^{-3} GeV$^{-1/2}$)	β_K	ϕ (deg.)	$\Delta\chi^2$ (%)
$S_{11}(1650)$ Fit 1	*1650*	*150*	27 ± 1	—	0.300 ± 0.033	228 ± 8	12.1
Fit 2	*1650*	*150*	3 ± 1	—	0.300 ± 0.283	119 ± 22	0.1
Fit 3	*1650*	*150*	23 ± 1	—	0.300 ± 0.001	192 ± 4	2.2
(****) PDG	1650	150	53 ± 16	—	0.027	—	—
$S_{11}(2090)$ Fit 1	2261 ± 15	241 ± 33	39 ± 2	—	0.096 ± 0.010	55 ± 7	5.0
Fit 2	2411 ± 12	377 ± 25	63 ± 4	—	0.044 ± 0.005	37 ± 5	5.6
Fit 3	2492 ± 10	500 ± 9	46 ± 3	—	0.173 ± 0.022	81 ± 3	4.5
(*) PDG	2090	400	—	—	—	—	—
$P_{11}(1710)$ Fit 1	1709 ± 13	150 ± 56	22 ± 6	—	0.019 ± 0.010	189 ± 16	2.0
Fit 2	1720 ± 3	150 ± 5	98 ± 4	—	0.010 ± 0.052	191 ± 2	2.5
Fit 3	1720 ± 2	150 ± 39	30 ± 3	—	0.029 ± 0.008	183 ± 4	2.3
(***) PDG	1710	100	9 ± 22	—	0.050	—	—
$P_{11}(2100)$ Fit 1	2129 ± 19	90 ± 20	-3 ± 1	—	0.289 ± 0.215	244 ± 40	0.8
Fit 2	2102 ± 4	90 ± 4	5 ± 1	—	0.300 ± 0.152	0 ± 0	3.8
Fit 3	2104 ± 4	90 ± 12	11 ± 3	—	0.029 ± 0.014	0 ± 5	1.5
(*) PDG	2100	200	—	—	—	—	—
$P_{13}(1720)$ Fit 1	*1720*	*150*	-22 ± 1	-20 ± 2	0.300 ± 0.053	46 ± 3	8.4
Fit 2	*1720*	*150*	-54 ± 3	-49 ± 2	0.097 ± 0.008	136 ± 2	4.7
Fit 3	*1720*	*150*	-31 ± 3	-22 ± 2	0.248 ± 0.042	84 ± 3	7.1
(****) PDG	1720	150	18 ± 30	-19 ± 20	—	—	—
$P_{13}(1900)$ Fit 1	1937 ± 7	102 ± 24	43 ± 5	-24 ± 13	0.011 ± 0.001	240 ± 12	4.4
Fit 2	1800 ± 5	500 ± 15	69 ± 2	88 ± 1	0.203 ± 0.007	208 ± 1	6.1
Fit 3	1818 ± 12	363 ± 29	194 ± 5	52 ± 10	0.011 ± 0.001	165 ± 6	2.9
(**) PDG	1900	498	—	—	0.001	—	—
$D_{13}(1700)$ Fit 1	1680 ± 3	170 ± 30	13 ± 1	18 ± 2	0.300 ± 0.027	110 ± 8	9.7
Fit 2	1750 ± 45	500 ± 385	56 ± 4	93 ± 4	0.010 ± 0.060	36 ± 2	3.6
Fit 3	1682 ± 3	499 ± 20	42 ± 2	69 ± 3	0.010 ± 0.001	37 ± 2	1.7
(***) PDG	1700	100	-18 ± 13	-2 ± 24	—	—	—
$D_{13}(2080)$ Fit 1	1936 ± 10	301 ± 22	-26 ± 2	-32 ± 3	0.300 ± 0.063	54 ± 7	8.8
Fit 2	1915 ± 4	165 ± 8	-140 ± 7	32 ± 4	0.012 ± 0.001	1 ± 3	8.5
Fit 3	1911 ± 4	193 ± 9	-85 ± 2	28 ± 3	0.034 ± 0.002	8 ± 3	7.1
(**) PDG	2080	450	-20 ± 8	17 ± 11	0.002	—	—
$D_{15}(1675)$ Fit 1	*1675*	*150*	22 ± 3	30 ± 3	0.010 ± 0.008	243 ± 7	4.2
Fit 2	*1675*	*150*	-2 ± 0	-15 ± 1	0.164 ± 0.029	212 ± 3	7.4
Fit 3	*1675*	*150*	0 ± 1	-13 ± 1	0.226 ± 0.015	203 ± 3	3.3
(****) PDG	1675	150	19 ± 8	15 ± 9	—	—	—
$D_{15}(2200)$ Fit 1	2247 ± 13	90 ± 10	-15 ± 2	3 ± 4	0.026 ± 0.006	108 ± 29	1.7
Fit 2	2299 ± 177	358 ± 41	-13 ± 4	-31 ± 5	0.038 ± 0.012	39 ± 11	2.6
Fit 3	2125 ± 17	500 ± 34	-41 ± 2	-19 ± 3	0.050 ± 0.007	6 ± 5	3.4
(**) PDG	2200	130	—	—	—	—	—
$F_{15}(1680)$ Fit 1	*1680*	*130*	-11 ± 4	11 ± 2	0.010 ± 0.014	190 ± 7	5.8
Fit 2	*1680*	*130*	-17 ± 1	15 ± 1	0.010 ± 0.006	5 ± 2	6.0
Fit 3	*1680*	*130*	-11 ± 1	25 ± 1	0.011 ± 0.001	27 ± 3	3.4
(****) PDG	1680	130	-15 ± 6	133 ± 12	—	—	—
$F_{15}(2000)$ Fit 1	2100 ± 9	345 ± 69	116 ± 25	36 ± 12	0.010 ± 0.001	208 ± 6	6.8
Fit 2	1937 ± 4	153 ± 10	53 ± 4	-14 ± 3	0.031 ± 0.005	0 ± 17	4.5
Fit 3	1967 ± 7	213 ± 15	33 ± 3	-61 ± 5	0.020 ± 0.002	55 ± 5	4.5
(**) PDG	2000	490	—	—	—	—	—
$F_{17}(1990)$ Fit 1	1970 ± 15	169 ± 30	-21 ± 4	-19 ± 5	0.040 ± 0.010	61 ± 9	2.7
Fit 2	2083 ± 15	531 ± 44	-12 ± 1	-15 ± 1	0.300 ± 0.285	72 ± 3	8.0
Fit 3	2056 ± 17	394 ± 48	-17 ± 1	-10 ± 1	0.233 ± 0.027	45 ± 6	4.7
(**) PDG	1990	535	30 ± 29	86 ± 60	—	—	—
$G_{17}(2190)$ Fit 1	*2190*	*450*	-6 ± 2	-14 ± 3	0.300 ± 0.252	27 ± 252	2.1
Fit 2	*2190*	*450*	-7 ± 1	14 ± 1	0.300 ± 0.272	10 ± 3	4.9
Fit 3	*2190*	*450*	-7 ± 1	26 ± 3	0.102 ± 0.022	6 ± 5	3.8
(****) PDG	2190	450	-55	81	—	—	—
$G_{19}(2250)$ Fit 1	*2250*	*400*	-20 ± 8	-18 ± 11	0.020 ± 0.018	153 ± 13	1.6

TABLE VI. *(Continued.)*

Resonance (status)	M_R (MeV)	Γ_R (MeV)	$A_{1/2}$ (10^{-3} GeV$^{-1/2}$)	$A_{3/2}$ (10^{-3} GeV$^{-1/2}$)	β_K	ϕ (deg.)	$\Delta\chi^2$ (%)
Fit 2	*2250*	*400*	6 ± 1	3 ± 1	0.300 ± 0.227	75 ± 7	1.9
Fit 3	*2250*	*400*	9 ± 1	-1 ± 1	0.300 ± 0.194	100 ± 5	3.7
(****) PDG	2250	400	—	—	—	—	—

same value of χ^2 the extracted β_K is 0.387 ± 0.150, which indicates that this resonance is still important for Fit 2.

Because the CLAS and SAPHIR data are binned in different energy and angular bins, a simultaneous comparison of the results with both data sets in one figure cannot be performed. In Figs. 3 and 4 we show the comparison between predictions from all fits with the CLAS data, whereas the comparisons with SAPHIR data are shown in Figs. 5 and 6. The LEPS data are shown in both cases. It is obvious from those figures that the LEPS data are more consistent with the CLAS data than with the SAPHIR measurement. This emphasizes the previous discussion on the numerical result of Table IV. From the four figures it is also clear that the largest discrepancy appears between $W = 1.75$ and 1.95 GeV in the forward direction, whereas in the backward direction the discrepancies show up in a wider range, i.e., from 1.8 to 2.4 GeV. It is also important to note that at the very forward and backward angles the two data sets (also, as a consequence, Fit 1 and Fit 2) exhibit very different trends. The CLAS data tend to rise at these regions, whereas the SAPHIR data tend to decrease.

The Λ recoil polarizations obtained from all fits are compared with experimental data in Fig. 7. Except at higher energies and in backward directions, where experimental data have large error bars, no result shows any significant difference. Therefore, in view of the present error bars, the Λ recoil polarization is not a decisive observable for revealing further information from the three fits. The energy distribution of this observable shown in Fig. 8 emphasizes this argument. At $\cos\theta = 0.5$ it is interesting to remark that the polarizations predicted by the three fits are almost similar and the values are

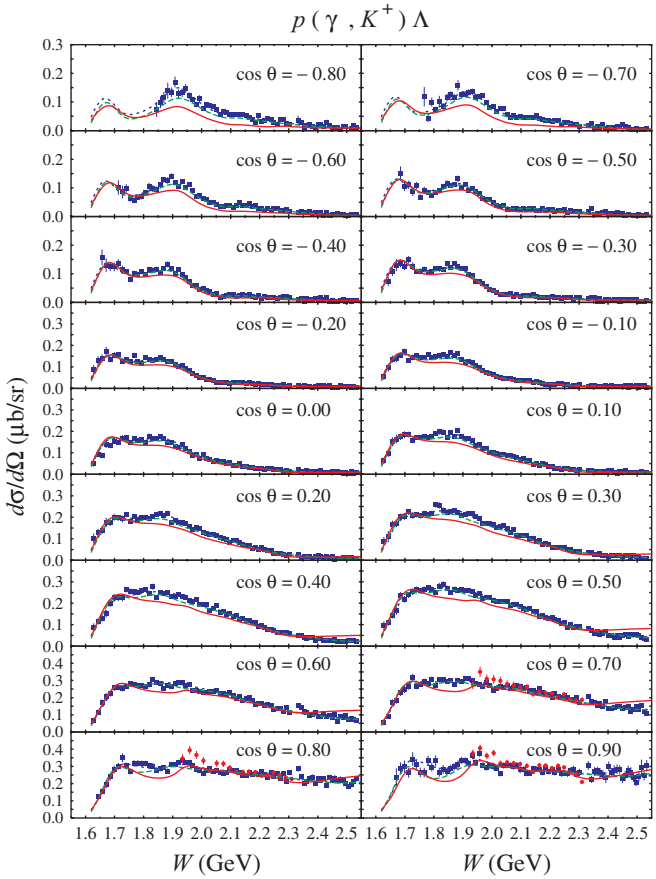

FIG. 4. (Color online) Same as in Fig 3, but for the energy distribution.

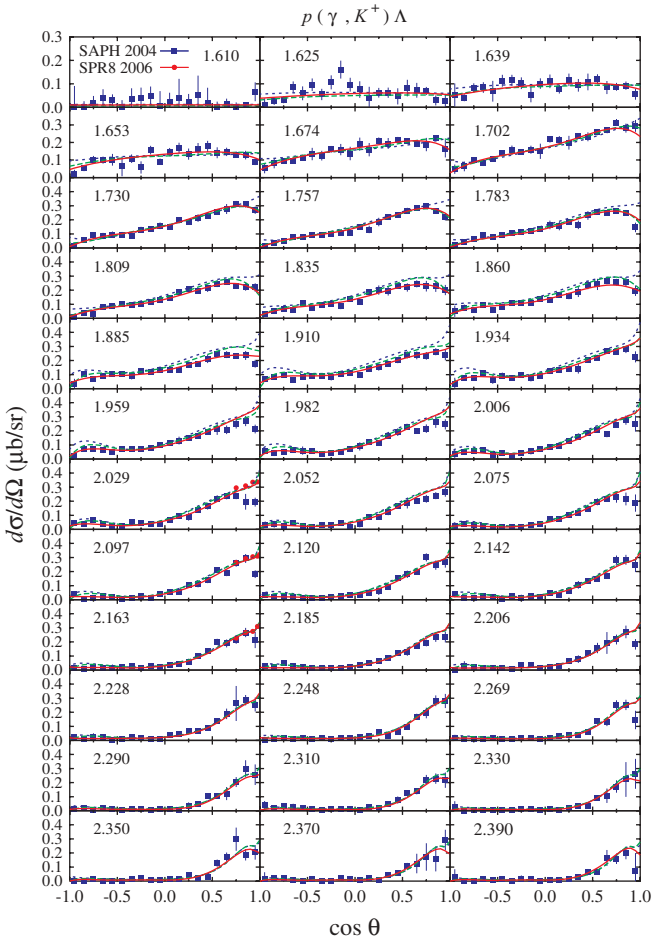

FIG. 5. (Color online) Comparison between angular distribution of differential cross sections obtained from the three fits with SAPHIR and LEPS data. Notation for the curves is the same as in Fig. 3.

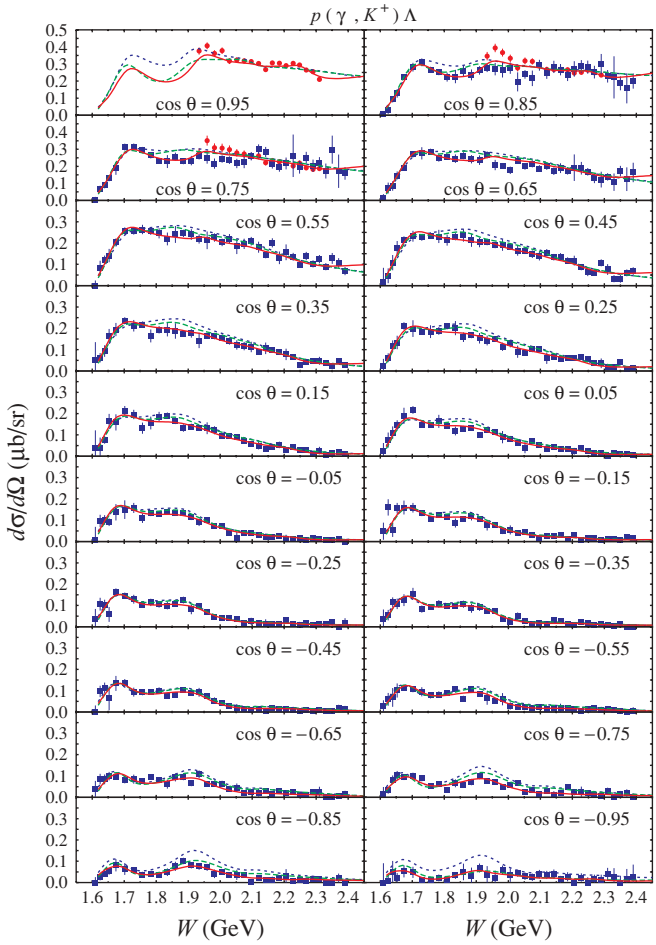

FIG. 6. (Color online) Same as in Fig 5, but for the energy distribution.

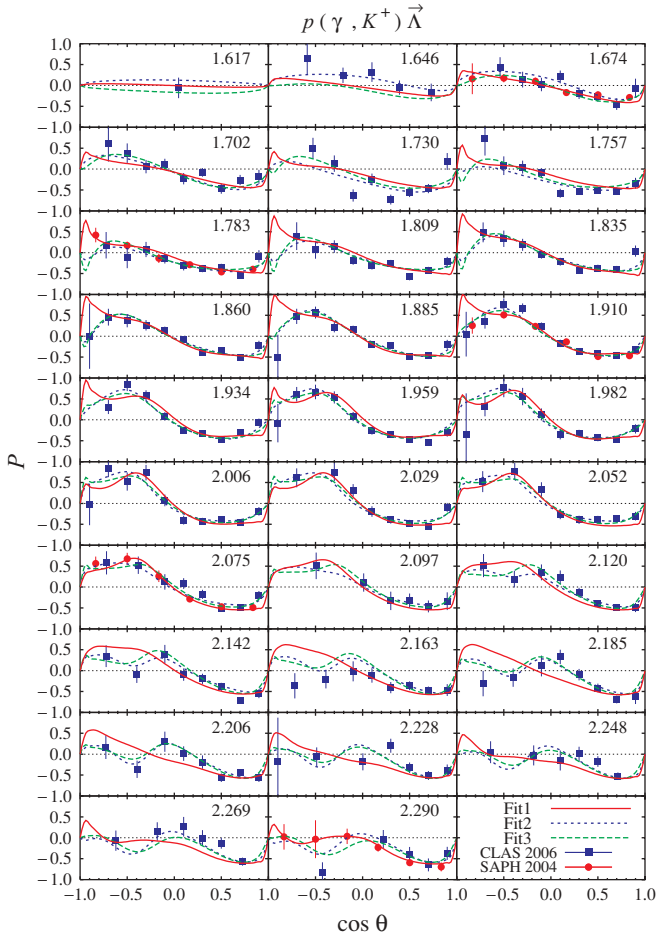

FIG. 7. (Color online) Comparison between the Λ recoil polarization obtained from the three fits with CLAS and SAPHIR data.

almost constant at about −0.5 over the whole energy range, except very close to threshold.

Both CLAS and SAPHIR Collaborations extracted the total cross sections and displayed them graphically. The numerical data points shown in Fig. 9 were taken from total cross-section figures of Refs. [17,18] and, for the sake of consistency, not used in the fits. In Ref. [7] it was suspected that the two collaborations have extracted the total cross sections in different ways, hence the discrepancy between them seems to be larger than that in differential cross sections. However, by comparing the solid line and solid squares, as well as the dotted line and solid circles in Fig. 9, we conclude that the extracted total cross sections from both collaborations are consistent with their differential cross sections. The fact that the discrepancy is more profound in the total cross sections is seemingly due to the cumulative effect of the integration, which can be immediately comprehended if we compare the solid lines (fit to the SAPHIR data) with dotted lines (fit to the CLAS data) in Fig. 4. However, the result of Fit 3 (dashed line in Fig. 9) clearly indicates that including both data sets in the fit results in a model that is consistent with no data set, as has been previously pointed out by Ref. [19].

The result for the polarized photon beam asymmetry is shown in Fig. 10, where we can obviously see a good agreement between predictions of all fits and the experimental data from LEPS. This result also corroborates the finding of Ref. [7] that further measurements of this observable in the backward directions would put a strong constraint on the model. Reference [7] found that the currently available experimental data of this observable (see the last line of Table IV) generate about 13% of the total χ^2. In contrast to this, we found that the data contribute only 3% (2%) to the total χ^2 of Fit 1 (Fit 2), which shows a better agreement of the three fits compared to models $M1$ and $M2$ of Ref. [7].

In Fig. 11 we compare the target asymmetry predicted by the three fits with experimental data. There are only three data points with large error bars available for this observable. To our knowledge, except for the Saclay-Lyon model [14], which is in only fair agreement with those data, other models [7,35,36] fail to reproduce them. Figure 11 clearly indicates that this observable could provide a stringent constraint to phenomenological models that try to explain the $K^+\Lambda$ photoproduction process. At this stage, it is important to note that we also obtained another solution for Fit 2 that can nicely reproduce these three data points. However, because the extracted parameters are quite different from those of Fit 1 and Fit 3 (as well as from the PDG values) and the corresponding $\chi^2 = 1610$ is slightly larger than that of Fit 2 (i.e., $\chi^2 = 1581$),

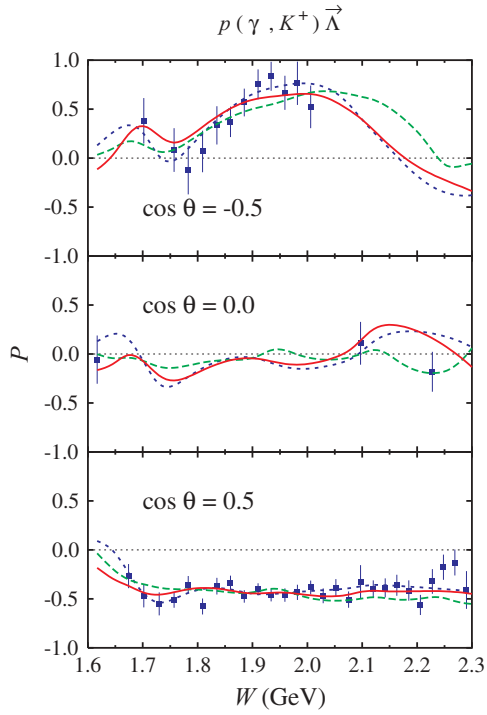

FIG. 8. (Color online) Same as in Fig. 7, but for the W distributions.

we do not follow up this alternative. Moreover, the number of available data and the size of error bars make it difficult to draw a firm conclusion on the discrepancy shown in Fig. 11. Future measurement of this asymmetry from threshold up to $W \approx 2.2$ GeV with error bars comparable to those of CLAS and SAPHIR data would certainly help to clarify this issue.

In Fig. 12 we display the multipole amplitudes for $\ell \leqslant 3$. It is obvious from this figure that the predicted multipoles are different in most cases, as has been also pointed out by Ref. [20]. This again indicates that the problem of mutual consistency in the presently available data still prohibits a more model-independent multipole analysis in kaon photoproduction.

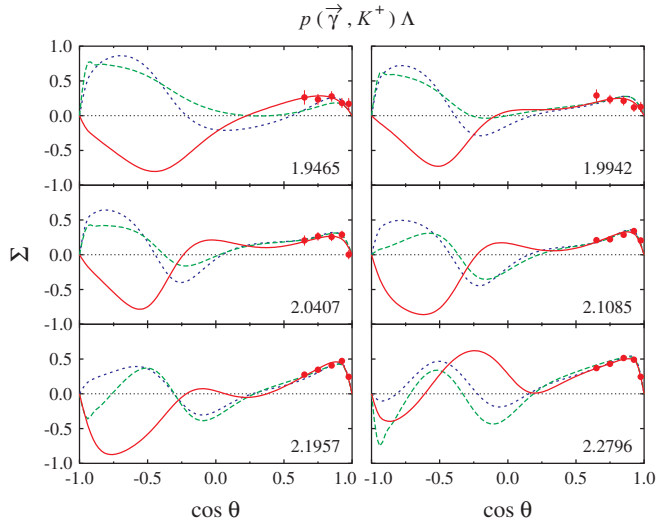

FIG. 10. (Color online) Photon asymmetry obtained from the three fits compared with the LEPS data. Notation for the curves is the same as in Fig. 3.

B. The first peak at $W \approx 1.7$ GeV

Both SAPHIR and CLAS data show an obvious peak at W around 1.7 GeV in the total as well as differential cross sections. Because these two data sets seem to be similar up to $W \approx 1.7$ GeV, it is reasonable to expect a similar resonance behavior below this energy region. However, Table VI indicates that, except for the $P_{13}(1720)$ and $F_{15}(1680)$, the two data sets require different resonances. This is elucidated in Fig. 13, where we compare the contribution of relevant resonances with masses around 1.7 GeV to the total cross section.

Due to their large $\Delta\chi^2$, contributions from the $S_{11}(1650)$, $P_{13}(1720)$, and $D_{13}(1700)$ in the case of Fit 1

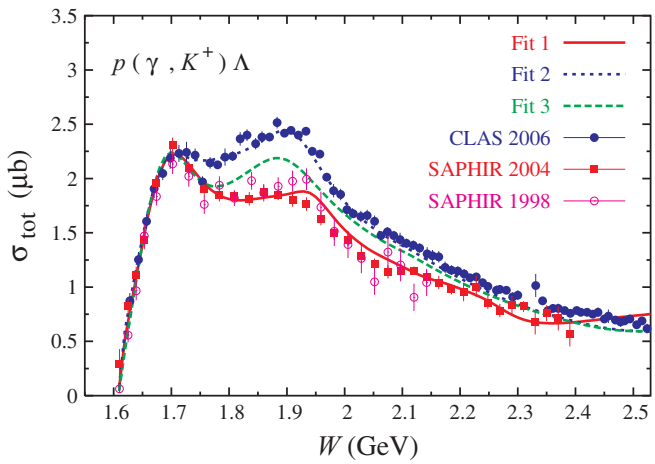

FIG. 9. (Color online) Comparison between the calculated total cross sections with experimental data. All data shown in this figure were not used in the fits.

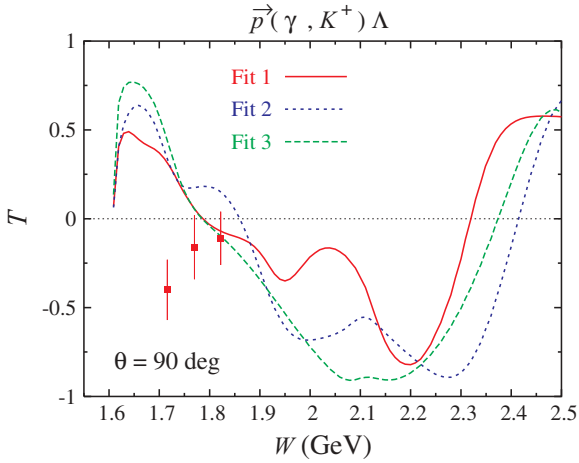

FIG. 11. (Color online) Comparison between target asymmetries obtained from the three different fits and experimental data [34]. Note that the three data points were not used in the fits.

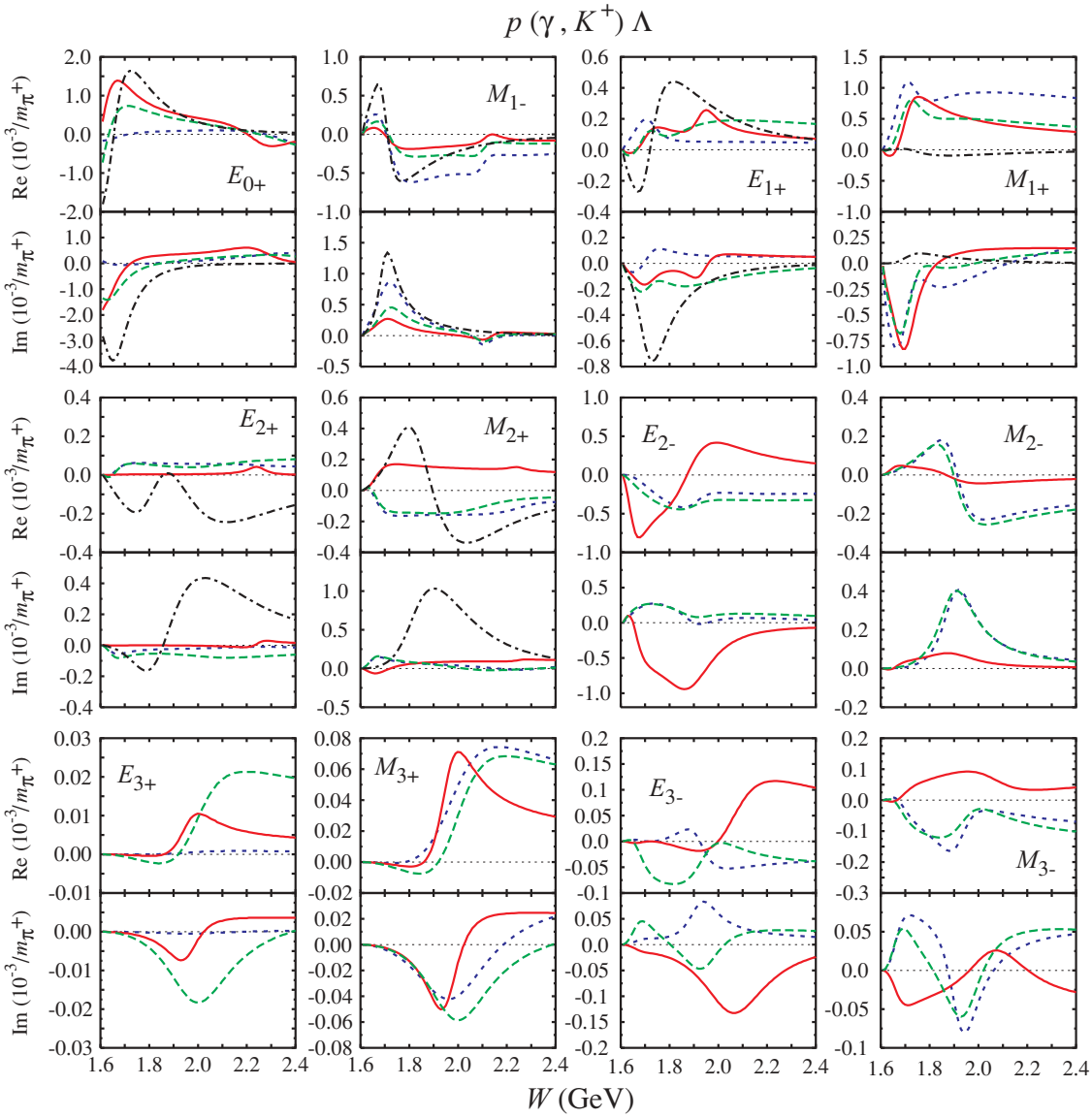

FIG. 12. (Color online) Electric and magnetic multipoles obtained from the three fits. The dash-dotted curves show the prediction of Kaon-Maid. Notation for other curves is the same as described in the legend to Fig. 3.

(the two upper panels of Fig. 13) are easily comprehended. The $F_{15}(1680)$ contribution, which, according to Table VI, is also important, is found to be important in describing the SAPHIR data only at the very forward angles. As a consequence, its contribution is difficult to see in this figure.

In contrast to the previous case, contributions of these resonances are somewhat complicated in the case of Fit 2 (the two lower panels of Fig. 13). This is mainly due to the relatively large background of the Fit 2 (see Fig. 1). Nevertheless, contributions from the $P_{13}(1720)$, $D_{15}(1675)$, and $F_{15}(1680)$ are still sizable. These contributions are required to decrease the cross section down to the experimental value through destructive interference.

The above result is clearly unexpected. However, we can understand this by carefully examine the total cross section data shown in Fig. 9 or the differential cross section data shown in Figs. 4 and 6, where we can see that at $W = 1.7$ GeV the discrepancy between the two data sets starts to appear. Given that the lowest-lying resonance used in this analysis is the $S_{11}(1650)$, which has a width of 150 MeV, all experimental data up to $W = 1.8$ GeV will certainly influence the extracted resonance parameters.

Another possible origin of the above finding is that the two data sets are already different for $W \lesssim 1.7$ GeV. To investigate this, we separately fitted both SAPHIR and CLAS differential cross sections data from threshold up to $W \approx 1.7$ GeV, by including the $S_{11}(1650)$, $P_{11}(1710)$, $P_{13}(1720)$, $D_{13}(1700)$, $D_{15}(1675)$, and $F_{15}(1680)$ resonances. We found that the extracted resonance parameters from the two fits are quite different, which, therefore, confirms that the two data sets are already different at $W \lesssim 1.7$ GeV.

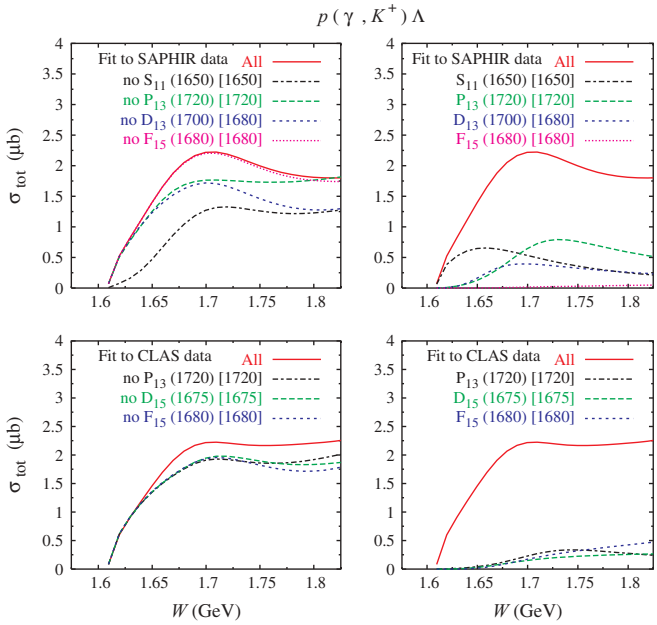

FIG. 13. (Color online) Contribution from resonances with masses around 1700 MeV to the total cross sections in the case of Fit 1 (upper panels) and Fit 2 (lower panels). For comparison, values of the extracted masses are shown in the square brackets.

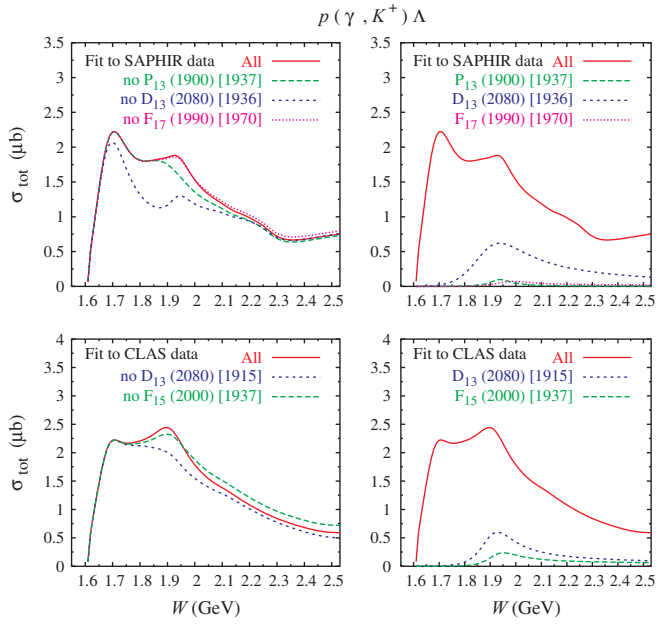

FIG. 14. (Color online) Same as Fig. 13, except for the resonances with masses around 1900 MeV, which contribute to the second peak in the total cross sections.

C. The second peak at $W \approx 1.9$ GeV

For almost one decade since the previous SAPHIR data were published in 1998 [39] there has been a lot of discussion on which resonance is responsible for explaining the second peak at $W \approx 1.9$ GeV in the total as well as differential cross sections. Here, it is important to note that, although varying as a function of the kaon angle in the latter case, the peak still exists in both CLAS and SAPHIR data.

The debate was ignited by the authors of Ref. [36], who, by means of the results from a certain constituent quark model [40] and an isobar model, interpreted the peak as the existence of the missing resonance $D_{13}(1895)$. Subsequently, it was shown by Janssen *et al.* [41] that the peak could be also equally well reproduced by including a $P_{13}(1950)$ resonance. However, most of analyses based on the isobar model after that confirmed that including the $D_{13}(1895)$ will significantly improve the agreement with experimental data [42].

A recent partial-wave analysis by Anisovich *et al.* [43] found that a new D_{13} with $M = 1875 \pm 25$ MeV and $\Gamma = 80 \pm 20$ MeV is needed to explain the processes $\gamma p \to \pi N, \eta N, K\Lambda$, and $K\Sigma$. Experimental data on the $\gamma p \to N^*(\Delta^*) \to \pi^0 p$ published by CB-ELSA Collaboration not long after that shifted this resonance to a higher mass, i.e., $M = 1943 \pm 17$ MeV and $\Gamma = 82 \pm 20$ MeV [44]. By analyzing the new SAPHIR data within a multipole approach Ref. [20] found that the D_{13} could have a mass and width of 1912 and 148 MeV (Model II of Table 1 in Ref. [20]). Meanwhile, a very recent coupled-channels analysis for the $\pi N \to KY$ and $\gamma N \to KY$ processes puts this resonance at $M = 1912$ MeV (or 1954 MeV) and $\Gamma = 316$ MeV (or 249 MeV), depending on the data set used in the fit [7]. Therefore, the obvious question is whether the second peak near $W \approx 1900$ MeV signals a D_{13} resonance with a mass of around 1900 MeV.

To answer this question let us look at Fig. 14, where we show the comparison between total cross sections of both Fit 1 and Fit 2 obtained by including all resonances and those obtained by excluding resonances with masses around 1900 MeV in the left panels. In the right panels a comparison between total cross sections obtained by including all resonances and those obtained from the individual resonances is shown. In the case of Fit 1 (upper panels), it is obvious that the $D_{13}(2080)$ with a mass of 1936 MeV provides the dominant contribution to this second peak. This can also immediately be seen from Fig. 2 or from Table VI, where we see that the corresponding $\Delta\chi^2 = 8.8\%$ is larger than that of the $P_{13}(1900)(4.4\%)$ or the $F_{17}(1990)\,(2.7\%)$. Albeit using a different formalism, this result is consistent with our previous finding [20], as well as with various analyses [7,44]. The reason that the mass of this D_{13} is shifted toward a higher value compared with the previous observation (1895 MeV as obtained in Ref. [36]) seemingly originates from the new SAPHIR data [17], which have the second peak at higher W compared with the previous ones [39] (see Fig. 6).

Interestingly, as shown by Fig. 2 and Table VI, the new CLAS data yield the same conclusion. Using this data set (Fit 2) the extracted mass of D_{13} is 1915 MeV, which is very close to the value given by Fit 1 (1936 MeV). As shown by Fig. 2 this resonance appears to be quite decisive in the process ($\Delta\chi^2 = 8.5\%$), and from the lower-left panel of Fig. 14 it is obvious that excluding this resonance in the process drastically changes the shape of the cross section. We also note that including all data sets in the fit does not change this conclusion.

To summarize this subsection we may say that within this multipole approach the two data sets lead to the same conclusion on the origin of the second peak in the W distribution of the cross sections, i.e., the $D_{13}(2080)$ with a mass between 1911 and 1936 MeV.

V. CONCLUSIONS AND OUTLOOK

We have analyzed the $\gamma p \to K^+\Lambda$ process by means of a multipole approach with a gauge-invariant, crossing-symmetric background amplitude obtained from tree-level Feynman diagrams. The corresponding free parameters are fitted to three different data sets, i.e., combinations of SAPHIR and LEPS data, CLAS and LEPS data, and all of these data. Results of the fit indicate the lack of mutual consistency between SAPHIR and CLAS data, whereas the LEPS data are shown to be more consistent with the CLAS ones. In most cases, the extracted parameters from the three data sets are found to be different and, therefore, could lead to different conclusions if those data were used individually or simultaneously to extract the information on missing resonances.

From a fit to SAPHIR and LEPS data it is found that the $S_{11}(1650)$, $P_{13}(1720)$, $D_{13}(1700)$, $D_{13}(2080)$, $F_{15}(1680)$, and $F_{15}(2000)$ resonances are more important than other resonances used in this analysis, whereas fitting to the combination of CLAS and LEPS data indicates that the $P_{13}(1900)$, $D_{13}(2080)$, $D_{15}(1675)$, $F_{15}(1680)$, and $F_{17}(1990)$ resonances are more decisive ones. It is shown that fitting to all data simultaneously changes this conclusion and results in a model that is inconsistent to all data sets.

Our analysis indicates that the target asymmetry cannot be described by any of the models. In view of the current available experimental data we conclude that measurement of this observable should be addressed in a future experimental proposal.

The three-star resonance $P_{11}(1710)$ that has been used in almost all isobar models within both single-channel and multichannel approaches is found to be insignificant to the $K^+\Lambda$ photoproduction by both SAPHIR and CLAS data.

It is also found that the second peak in cross sections at $W \sim 1900$ MeV originates from the $D_{13}(2080)$ resonance. The extracted mass would be 1936 MeV if SAPHIR data were used or 1915 MeV if CLAS data were used. This finding would not change if all data sets were used.

We have observed that the total cross sections reported by the two collaborations are consistent with their differential cross sections. The fact that the discrepancy is larger in the total cross sections stems from the cumulative effect of the integration.

Although results of the present work could reveal certain consequences of using SAPHIR or CLAS data in the database, it is still difficult to determine which data set should be used to obtain the correct resonance parameters. We also realize that the results presented here are not final, because a more representative calculation should ideally be performed in a coupled-channels formalism where other channels such as πN, ηN, $\pi\pi N$, and ωN are also taken into account. Nevertheless, the simple calculation presented here has revealed two most important issues that will need to be addressed in future calculations: (1) contribution from higher spin resonances are important and (2) until we can settle the problem of data consistency, the results of all calculations are now data dependent. Future measurements such as the one planned at MAMI in Mainz are, therefore, expected to remedy this unfortunate situation.

Our next goal is to consider the $\gamma p \to K^+\Sigma^0$ channel and to incorporate the effect of other related channels.

ACKNOWLEDGEMENT

The authors thank William J. Briscoe for carefully reading the manuscript and acknowledge the support from the Faculty of Mathematics and Sciences, University of Indonesia, as well as from the Hibah Pascasarjana grant.

[1] R. A. Adelseck, C. Bennhold, and L. E. Wright, Phys. Rev. C **32**, 1681 (1985).
[2] R. A. Adelseck and B. Saghai, Phys. Rev. C **42**, 108 (1990).
[3] R. A. Williams, C. R. Ji, and S. R. Cotanch, Phys. Rev. C **43**, 452 (1991).
[4] B. S. Han, M. K. Cheoun, K. S. Kim, and I. T. Cheon, Nucl. Phys. **A691**, 713 (2001).
[5] T. Mart, C. Bennhold, H. Haberzettl, and L. Tiator, Kaon-Maid, available at http://www.kph.uni-mainz.de/MAID/kaon/kaonmaid.html. The published versions are available in Ref. [36]; T. Mart, Phys. Rev. C **62**, 038201 (2000); C. Bennhold, H. Haberzettl, and T. Mart, arXiv:nucl-th/9909022.
[6] T. Feuster and U. Mosel, Phys. Rev. C **59**, 460 (1999).
[7] B. Julia-Diaz, B. Saghai, T. S. H. Lee, and F. Tabakin, Phys. Rev. C **73**, 055204 (2006).
[8] W. T. Chiang, F. Tabakin, T. S. H. Lee, and B. Saghai, Phys. Lett. **B517**, 101 (2001).
[9] Z. Li, Phys. Rev. C **52**, 1648 (1995).
[10] D. Lu, R. H. Landau, and S. C. Phatak, Phys. Rev. C **52**, 1662 (1995).
[11] T. Mart and T. Wijaya, Acta Phys. Polon. B **34**, 2651 (2003).
[12] T. Mart and C. Bennhold, arXiv:nucl-th/0412097.
[13] T. Corthals, J. Ryckebusch, and T. Van Cauteren, Phys. Rev. C **73**, 045207 (2006).
[14] J. C. David, C. Fayard, G. H. Lamot, and B. Saghai, Phys. Rev. C **53**, 2613 (1996).
[15] F. M. Renard and Y. Renard, Nucl. Phys. **B25**, 490 (1971); Y. Renard, *ibid*. **B40**, 499 (1972); Thèse de Doctorat d'Etat ès-Sciences Physiques, Université des Sciences et Techniques du Languedoc, 1971 (unpublished).
[16] S. Eidelman *et al*. (Particle Data Group), Phys. Lett. **B592**, 1 (2004).
[17] K. H. Glander *et al*., Eur. Phys. J. A **19**, 251 (2004).
[18] R. Bradford *et al*. (CLAS Collaboration), Phys. Rev. C **73**, 035202 (2006).
[19] P. Bydzovsky and T. Mart, arXiv:nucl-th/0605014.

[20] T. Mart, A. Sulaksono, and C. Bennhold, arXiv:nucl-th/0411035.
[21] D. Drechsel, O. Hanstein, S. S. Kamalov, and L. Tiator, Nucl. Phys. **A645**, 145 (1999).
[22] L. Tiator, D. Drechsel, S. Kamalov, M. M. Giannini, E. Santopinto, and A. Vassallo, Eur. Phys. J. A **19**, 55 (2004).
[23] The explicit expression for the background amplitudes are given, e.g., in Ref. [11], or in T. Mart, Ph.D thesis, Universität Mainz, 1996 (unpublished).
[24] H. Thom, Phys. Rev. **151**, 1322 (1966).
[25] R. A. Adelseck and L. E. Wright, Phys. Rev. C **38**, 1965 (1988).
[26] K. Ohta, Phys. Rev. C **40**, 1335 (1989).
[27] R. M. Davidson and R. Workman, Phys. Rev. C **63**, 025210 (2001).
[28] H. Haberzettl, C. Bennhold, T. Mart, and T. Feuster, Phys. Rev. C **58**, R40 (1998).
[29] W. T. Chiang, S. N. Yang, L. Tiator, and D. Drechsel, Nucl. Phys. **A700**, 429 (2002).
[30] I. G. Aznauryan, Phys. Rev. C **67**, 015209 (2003).
[31] G. Knochlein, D. Drechsel, and L. Tiator, Z. Phys. A **352**, 327 (1995).
[32] J. W. C. McNabb *et al.* (The CLAS Collaboration), Phys. Rev. C **69**, 042201 (2004); J. W. C. McNabb, Ph.D. thesis, Carnegie Mellon University, 2002; R. Schumacher (private communication).
[33] M. Sumihama *et al.* (LEPS Collaboration), Phys. Rev. C **73**, 035214 (2006).
[34] K. H. Althoff *et al.*, Nucl. Phys. **B137**, 269 (1978).
[35] O. V. Maxwell, Phys. Rev. C **70**, 044612 (2004).
[36] T. Mart and C. Bennhold, Phys. Rev. C **61**, 012201(R) (1999).
[37] References for old measurements are listed in Table IX of Ref. [2], or in references of Ref. [39].
[38] T. Mart and L. Tiator (work in progress).
[39] M. Q. Tran *et al.* (SAPHIR Collaboration), Phys. Lett. **B445**, 20 (1998).
[40] S. Capstick and W. Roberts, Phys. Rev. D **49**, 4570 (1994); **58**, 074011 (1998); S. Capstick, *ibid.* **46**, 2864 (1992).
[41] S. Janssen, J. Ryckebusch, D. Debruyne, and T. Van Cauteren, Phys. Rev. C **65**, 015201 (2001).
[42] See, e.g.,T. K. Choi, M. K. Cheoun, K. S. Kim, and B. G. Yu, in *Proceedings of the International Symposium On Electrophoto-Production of Strangeness on Nucleons and Nuclei (SENDAI 03), 16–18 June 2003, Sendai, Japan,* edited by K. Maeda, H. Tamura, S. N. Nakamura, and O. Hashimoto (World Scientific, Singapore, 2004), pp. 85.
[43] A. V. Anisovich, A. Sarantsev, O. Bartholomy, E. Klempt, V. A. Nikonov, and U. Thoma, Eur. Phys. J. A **25**, 427 (2005).
[44] O. Bartholomy *et al.* (CB-ELSA Collaboration), Phys. Rev. Lett. **94**, 012003 (2005).